J. Plasma Physics (1996), *vol.* 56, *part* 3, *pp.* 641–657. Printed in the United Kingdom 641

Ion parallel viscosity and anisotropy in MHD turbulence

SEAN OUGHTON

Department of Mathematics, University College London,
Gower Street, London WC1E 6BT, UK

(Received 20 May 1996)

We report on results from direct numerical simulation of the incompressible three-dimensional magnetohydrodynamic (MHD) equations, modified to incorporate viscous dissipation via the strongly anisotropic ion-parallel viscosity term. Both linear and nonlinear cases are considered, all with a strong background magnetic field. It is found that spectral anisotropy develops in almost all cases, but that the contribution from effects associated with the ion-parallel viscosity is relatively weak compared to the previously reported nonlinear process. Furthermore, and in contrast to this earlier work, it is suggested that when $\mathbf{B}_0$ is large, the anisotropy will develop and persist for many large-scale turnover times even for non-dissipative runs. Resistive dissipation is found to dominate over viscous even when the resistivity is several orders of magnitude smaller than the ion parallel viscosity. A variance anisotropy effect and anisotropy dependence on the polarization of the fluctuations are also observed.

1. Introduction and Background

Anisotropies of various kinds are frequently, even typically, observed in magnetohydrodynamic (MHD) systems with a large-scale magnetic field $\mathbf{B}_0$. Examples include laboratory plasma devices, where spectral anisotropy is seen (Robinson and Rusbridge 1971; Zweben *et al.* 1979; Montgomery and Turner 1981), and the solar wind, for which observational evidence has been given for both spectral anisotropy (Matthaeus *et al.* 1990; Bieber *et al.* 1996) and variance anisotropy (Belcher and Davis 1971; Bavassano *et al.* 1982; Klein *et al.* 1991; Horbury *et al.* 1995).

On the theoretical side, Montgomery and Turner (1981) used perturbation theory, expanding in powers of $1/B_0$, to show that the leading-order MHD fluctuations are perpendicular to a strong magnetic field. Numerical support for this theory was provided by Shebalin *et al.* (1983) who performed simulations of the nonlinear dissipative two-dimensional (2D) MHD equations with a uniform $\mathbf{B}_0$. Their work showed that initially isotropic states evolved into strongly anisotropic ones. Specifically, they reported the development of anisotropy in the wavenumber spectra of the fluctuations and presented an explanation for this behaviour based on weak turbulence calculations of the leading-order nonlinear corrections to the linearized solutions (Alfvén waves).

The work of Shebalin *et al.* was recently extended to the three-dimensional (3D) case and, as they conjectured, essentially the same development of spectral anisotropy was observed (Oughton *et al.* (1994, 1995); however, see Sridhar and

Goldreich (1994) and Montgomery and Matthaeus (1995) for discussion on the relevance of the weak turbulence explanation). Two points should be noted regarding these simulations: (i) the anisotropy generation process is intrinsically nonlinear – linear runs show no tendency to develop anisotropy when viscosity and resistivity are equal; and (ii) dissipation (in the standard ∇^2 form) was necessary for the anisotropy to persist after its development, at least when $B_0 \approx 1$. Numerical work based on an MHD shell model (Carbone and Veltri 1990) also shows the development of spectral anisotropy, with a saturation occuring at Reynolds numbers of order 10^5.

While theory and simulations based on the incompressible MHD equations have shown that *spectral* anisotropy can be dynamically generated if a large enough $\mathbf{B}_0$ is present, any *variance* anisotropy which develops appears to be associated with an excess of parallel energy. This is counter to solar wind observations, where the perpendicular power dominates (Belcher and Davis 1971; Klein *et al.* 1991; Horbury *et al.* 1995). Motivated by these observational results, Matthaeus *et al.* (1996) performed a series of compressible (polytropic) MHD simulations. In addition to spectral anisotropy very similar to that seen in the incompressible runs, variance anisotropy was also observed to develop, and, moreover, was in qualitative agreement with solar wind data.

Thus it might appear that explanations for observed spectral and var-iance anisotropies have been found. However, it is not clear that the anisotropies must be generated via these mechanisms. In particular, the viscous and resistive terms were assumed to be of the isotropic (e.g. $\nabla^2\mathbf{v}$) form. Montgomery (1992) has emphasized that for a magnetofluid threaded by a strong large-scale magnetic field, it is questionable whether the appropriate viscous dissipation term is the usual isotropic Laplacian one. Instead, the standard transport coefficient calculations (Braginskii 1965; Book 1987) indicate that a term which is strongly anisotropic should be used in its place (the resistive term remaining unchanged). Under appropriate conditions (see Sec. 2) this term is proportional to a single scalar coefficient, the (kinematic) ion parallel viscosity, $\nu_{\rm ion}$, which may be interpreted as the product of the thermal speed and the collisional mean free path length parallel to $\mathbf{B}_0$.

Proceeding on this basis, Montgomery showed that solutions to the linearized equations could develop strong (spectral) anisotropy – even in the absence of spectral transfer, and suggested that this mechanism might be of importance for a variety of magnetofluids, including fusion plasmas and the solar wind.

Acting on this suggestion of Montgomery's, we report here on the first results from numerical simulations of the linear and nonlinear incompressible MHD equations modified to reflect the inclusion of the ion parallel viscosity term. In Sec. 2 we detail the approximations and equations employed and present some numerical details. Section 3 contains the theory for the linearized equations, while Sec. 4 discusses the numerical results. The paper closes with a summary of findings and our conclusions.

2. Equations and Approximations

In the general case, the well known Braginskii (1965) calculations for the MHD transport coefficients yield a viscosity tensor characterised by three classes of elements. However, when $\omega_c\tau \gg 1$, where ω_c is the ion cyclotron frequency and τ the

ion collision time, the viscous dissipation is dominated by terms proportional to the ion parallel viscosity, conventionally denoted by η_0 (see e.g. Montgomery 1992).

Under the further assumptions of incompressible flow and η_0 a uniform constant, the viscous term can be shown to reduce to

$$-\eta_0 \nabla \cdot \left\{ \left(\mathsf{I} - 3\hat{\mathbf{B}}\hat{\mathbf{B}} \right) \hat{\mathbf{B}}\hat{\mathbf{B}} : \nabla \mathbf{v} \right\}, \tag{2.1}$$

where $\hat{\mathbf{B}}$ is the unit vector in the direction of the (total) magnetic field. Such a term presents both analytical and computational difficulties; however, if $\mathbf{B}_0 = B_0 \hat{\mathbf{z}}$, is uniform and strong, then $\hat{\mathbf{B}} \approx \hat{\mathbf{B}}_0 = \hat{\mathbf{z}}$, which is a uniform constant. This approximation will be employed throughout the remainder of the paper. Using Cartesian coordinates, (2.1) then simplifies to

$$+\eta_0 \left(-\frac{\partial^2}{\partial x \partial z}, -\frac{\partial^2}{\partial y \partial z}, 2\frac{\partial^2}{\partial z^2} \right) v_z = \eta_0 \mathbf{D} v_z. \tag{2.2}$$

Note that in Fourier space only the z component of $\mathbf{D}$ is of definite sign. The error in the approximation $\hat{\mathbf{B}} = \hat{\mathbf{B}}_0$ can be crudely estimated to be of order b/B_0, where b is the rms magnetic fluctuation. In the simulations this ratio is initially $1/10$ and decreases throughout the runs, so that the validity of the approximation also increases with time.

Taking the mass density ρ to be uniform and constant, the associated kinematic viscosity coefficient is $\nu_{\text{ion}} = \eta_0/\rho$. Using values obtained from spacecraft data, Montgomery (1992) estimated that in the solar wind at 1 AU, for example, $\nu_{\text{ion}} \approx 10^{19}\,\text{cm}^2\,\text{s}^{-1}$, and $\omega_c \tau \approx 10^6$, which suggests that the above approximations may well be satisfied in this case. Using the same data, the (electron) resistivity is $\eta \approx 10^5\,\text{cm}^2\,\text{s}^{-1}$(Book 1987). Furthermore, for a typical solar wind velocity fluctuation (RMS) of $20\,\text{km}\,\text{s}^{-1}$, and a velocity correlation length of $5 \times 10^{11}\,\text{cm}$ (see e.g. Matthaeus and Goldstein 1982), the associated Reynolds number is $R_e = u\lambda_{\text{corr}}/\nu_{\text{ion}} \approx 10^{-1}$, which is certainly computationally accessible.

Under the assumptions just discussed, the (modified) incompressible 3D MHD equations can be written in the dimensionless form

$$\frac{\partial \mathbf{v}}{\partial t} + \mathbf{v} \cdot \nabla \mathbf{v} = -\nabla p^* + \mathbf{b} \cdot \nabla \mathbf{b} + \mathbf{B}_0 \cdot \nabla \mathbf{b} + \nu_{\text{ion}} \mathbf{D} v_z, \tag{2.3}$$

$$\frac{\partial \mathbf{b}}{\partial t} + \mathbf{v} \cdot \nabla \mathbf{b} = \mathbf{b} \cdot \nabla \mathbf{v} + \mathbf{B}_0 \cdot \nabla \mathbf{v} + \eta \nabla^2 \mathbf{b}, \tag{2.4}$$

$$\nabla \cdot \mathbf{v} = \nabla \cdot \mathbf{b} = 0, \tag{2.5}$$

where $\mathbf{v}$ and $\mathbf{b}$ are the zero-mean velocity and magnetic field fluctuations, p^* is the total pressure (mechanical plus magnetic), η the resistivity, and $\mathbf{D}$ is defined by (2.2). The numerical results were obtained via spectral (Galerkin) simulation of these equations in Fourier space using dealiasing and isotropic truncation. All runs are freely decaying. Note that because the viscous dissipation depends on gradients of v_z (not $\mathbf{v}$), the pressure gradient term cannot be satisfied using *only* the 'standard' projection operator form (see e.g. Orszag 1977, Lesieur 1990). Timestepping is performed using an explicit second-order Runge–Kutta method, with $\Delta t = \frac{1}{2000}$ in all $B_0 = 10$ runs. Since B_0 is large, the timestep must be small in order to adequately resolve the small-scale Alfvén waves. Units are such that $B_0^2 = 1$ corresponds to the fluctuations having the same initial energy as $\mathbf{B}_0$. Further computational details are available in Oughton *et al.* (1994)

Other quantities of relevance include the current density $\mathbf{j} = \nabla \times \mathbf{b}$, vorticity

Table 1. All runs have $B_0 = 10$ and $\sigma_c \approx 0$ unless otherwise noted. A dot indicates the value is the same as that listed above it. Runs 04–11 use the same initial Fourier coefficients. Similarly the run sets 15–17, and 18 and 20 use distinct initial Fourier coefficients. The linear runs of necessity have $\sigma_c \equiv 1$.

Run	η	ν_{ion}	k_L–k_H	$\alpha = 2B_0/3k\nu_{ion}$	Linear	Comments
04	10^{-2}	0	3–8	∞		$\nu = \eta$, 'standard dissipation'
05	10^{-2}	0	.	.		
06	0	0	.	.		Ideal run
07	0	10	.	0.7–0.04		
08	0	10^{-1}	.	70–4		
09	10^{-2}	10	.	0.7–0.04		
10	10^{-2}	10^{-1}	.	70–4		
11	0	10^{-2}	.	700–40		
15	0	10	1–15	0.7 – 0.04	Y	True linear solutions
16	10^{-2}	10	.	.	Y	
17	0	10^{-1}	.	70 – 4	Y	
18	0	10	9–15	0.08 – 0.04	Y	
19	0	10	3–8	0.2 – 0.09	Y	
20	0	10	9–15	0.08 – 0.04	Y	$B_0 = 15$, $\Delta t = \frac{1}{4000}$

$\boldsymbol{\omega} = \nabla \times \mathbf{v}$, kinetic and magnetic energies per unit mass $E^v = \langle \frac{1}{2}|\mathbf{v}|^2 \rangle$, $E^b = \langle \frac{1}{2}|\mathbf{b}|^2 \rangle$, total fluctuation energy $E = E^v + E^b$, and the cross helicity $H_c = \langle \mathbf{v} \cdot \mathbf{b} \rangle$. Angle brackets denote averaging over the spatial domain, and the time unit is the initial large-scale eddy-turnover time.

Also of considerable use are the (discrete) Fourier decompositions of the dependent variables, e.g. $\mathbf{v}(\mathbf{x}, t) = \sum_{\mathbf{k}} \mathbf{v}(\mathbf{k}, t)\, e^{\mathrm{i}\,\mathbf{k}\cdot\mathbf{x}}$. As the spatial domain is a cube of side 2π with periodic boundary conditions imposed, the wavevectors $\mathbf{k}$ have integer components. Modal spectra are denoted by $E^v(\mathbf{k})$ etc. (see e.g. Batchelor 1970). The runs discussed here retain 32 Fourier modes in each Cartesian direction. Table 1 contains a summary of the important run parameters.

3. Linear Theory

Linearizing (2.3)–(2.5) and seeking solutions for $\mathbf{v}$ and $\mathbf{b}$ of the form $e^{\mathrm{i}(\mathbf{k}\cdot\mathbf{x} - \omega t)}$ yields the linear dispersion relation

$$\left[\omega^2 + i\eta k^2 \omega - (\mathbf{k} \cdot \mathbf{B}_0)^2\right] \mathbf{v} = i\, 3\nu_{\mathrm{ion}} \cos^2\theta \left(\omega + i\eta k^2\right) \left(k_z \mathbf{k} - k^2 \hat{\mathbf{z}}\right), \qquad (3.1)$$

with $\cos\theta = \hat{\mathbf{k}} \cdot \hat{\mathbf{B}}_0$. Note that the contribution from the pressure term is non-zero. Forming the scalar product of (3.1) with $\mathbf{v}$ reveals that there are two cases (polarizations) to consider. First, when $v_z = 0$ the solution is as for the resistive but non-viscous situation, and propagating modes only occur for $k < |2B_0 \cos\theta/\eta|$. Thus near $\theta = 90^\circ$ only very long wavelength modes can propagate. Note that smaller resistivity is associated with less restrictive propagation conditions.

The second case is where $\mathbf{v}$ is in the $(\mathbf{k}, \mathbf{B}_0)$ plane with $v_z \neq 0$, and has solution,

$$\frac{2\omega}{k^2} = -i(\eta + 3\nu_{\mathrm{ion}} \cos^2\theta \sin^2\theta) \pm \sqrt{4B_0^2 k^{-2} \cos^2\theta - \left(\eta - 3\nu_{\mathrm{ion}} \cos^2\theta \sin^2\theta\right)^2}. \qquad (3.2)$$

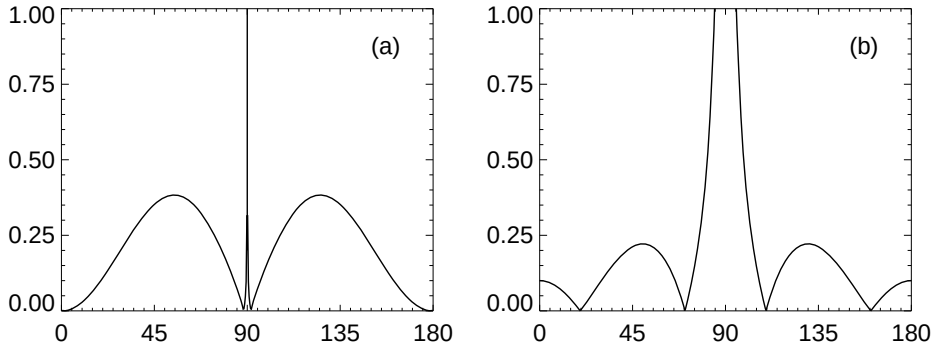

Figure 1. The left-hand side of (3.3) as a function of θ for (a) $\beta \equiv \nu_{\rm ion}/3\eta = 10^{-3}$; (b) $\beta = 10^{-1}$.

Propagating solutions must therefore satisfy

$$\frac{1}{|\cos\theta|}\left|\frac{\eta}{3\nu_{\rm ion}} - \cos^2\theta\sin^2\theta\right| < \frac{2B_0}{3k\nu_{\rm ion}} \quad = \alpha. \tag{3.3}$$

Montgomery (1992) obtained the $\eta = 0$ limits of these equations. Thus, if $\beta = \eta/3\nu_{\rm ion} \ll 1$ and α is small then (3.3) will only be satisfied for either $\theta \approx 0$ or $180°$, cones about the z–axis, or $\theta \approx 90°$, a wedge. On the other hand, if $\alpha \geq 1$ then (3.3) is essentially always satisfied, for small enough β, and no anisotropy from this source is expected. There are two special cases: fluctuations with $\mathbf{k}$ perpendicular or parallel to $\mathbf{B}_0$ suffer only resistive damping. Note that the numerator of α is intrinsically large because of the earlier approximation of large B_0.

When β is not much less than unity, however, the situation changes. Figure 1 displays plots of the left-hand side of (3.3) for two values of β. It can be seen that $\beta \neq 0$ introduces a spike at $\theta = 90°$, whose width increases as β does. Consequently, the viable propagation regimes are pushed away from the $\beta = 0$ viable regions, so that now only shells of θ values admit propagation. As can be seen in the plots, the effect is only significant for $\beta > 10^{-3}$, unless θ is extremely close to $90°$. Nonetheless, even for such small values of β the resistive dissipation mechanism can dominate over the viscous one, as will be shown below.

The solenoidal nature of $\mathbf{v}$ means it can be decomposed using a $\mathbf{k}$-dependent coordinate system:

$$\mathbf{v}(\mathbf{k}) = \mathbf{e}_1\psi_1 + \mathbf{e}_2\psi_2, \tag{3.4}$$

with $\mathbf{e}_1 = \mathbf{k}\times\hat{\mathbf{z}}/|\mathbf{k}\times\hat{\mathbf{z}}|$, $\mathbf{e}_2 = \mathbf{k}\times\mathbf{e}_1/|\mathbf{k}|$, and similarly $\mathbf{b}(\mathbf{k}) = \mathbf{e}_1 a_1 + \mathbf{e}_2 a_2$. We refer to these components as the $\mathbf{e}_1$ and $\mathbf{e}_2$ polarizations. When $\mathbf{k} \parallel \hat{\mathbf{z}}$, $\mathbf{e}_1$ and $\mathbf{e}_2$ are arbitrarily taken to be $\hat{\mathbf{x}}$ and $\hat{\mathbf{y}}$. Recall that $\hat{\mathbf{B}}_0 \equiv \hat{\mathbf{z}}$.

The condition $v_z(\mathbf{k}) = 0$ thus requires $\psi_2 \equiv 0$, and consequently the $\mathbf{e}_1$ polarization is completely unaffected by the viscous term. We might therefore anticipate that the $\mathbf{e}_2$ polarization will become more anisotropic than the $\mathbf{e}_1$ one (Montgomery 1992), even for the nonlinear runs. Furthermore, since the v_x and v_y components contain $\mathbf{e}_1$ contributions, but v_z does not, we anticipate that variance anisotropy will develop in the linear runs, with perpendicular power exceeding parallel. Both expectations are confirmed by the simulations.

Finally in this section, (3.3) indicates that the propagation condition becomes harder to satisfy at larger k, that is, the smaller scales are likely to be more

anisotropic, which is in agreement with solar wind observations (see e.g. Horbury *et al.* 1995). We return to this point in the discussion section.

4. Numerical Results

The results discussed below pertain to the runs listed in Table 1, all of which have $B_0 = 10$. Additionally, each initial condition set has $E^v(k) = E^b(k)$, with $E = 1$, and approximately zero kinetic and magnetic helicity. The initial Fourier coefficients are assigned so that the modal spectra are of the form $E^v(\mathbf{k}) \sim 1/[1 + (k/k_{\rm knee})^q]$, with $k_{\rm knee} = 4$, and q chosen so that the omnidirectional spectra have a high-wavenumber slope of the Kolmogorov value, $-\frac{5}{3}$. The phases for the coefficients are determined using Gaussian random variables, and only Fourier modes with wavenumbers in the range k_L to k_H are initially populated. Unfortunately, computational constraints – in particular the small time-steps required to resolve the small scale Alfvén waves – restricted us to relatively low resolution runs, with initial viscous and resistive Reynolds numbers, $R_e \equiv \nu_{\rm ion}^{-1}$, $R_m \equiv \eta^{-1}$, of at most a few hundred. Initial conditions for the linear runs have maximal cross helicity, i.e. $\mathbf{v}(\mathbf{k}) = \mathbf{b}(\mathbf{k})$, as required for consistency with the linear analysis.

Our approach has been to generate a specific set of initial data and then perform multiple runs with it, varying only $\nu_{\rm ion}$ and η from run to run. As indicated in Table 1, several such initial condition sets have been used. In the following we consider first the temporal evolution of bulk quantities like the turbulent energy density, and thereafter discuss the anisotropy behaviour. As will be seen, there are important differences between the η zero/non-zero results, even for $\eta \ll \nu_{\rm ion}$.

4.1. Bulk Properties

Figure 2(a) displays plots of the fluctuation energy $E(t)$ for four typical runs. Consider first the $\eta = 0$ runs 07 and 08. It is apparent that as far as energy dissipation is concerned, ion parallel viscous effects are relatively weak, when compared with the energy decay associated with standard Laplacian viscous terms (see also Shebalin *et al.* 1983; Oughton *et al.* 1994). Indeed, for runs with $\nu_{\rm ion} \lesssim 10^{-1}$ plots of the globals and other diagnostics are indistinguishable from those for ideal runs (e.g. run 06). Thus, somewhat counter-intuitively, even low-(ion parallel) Reynolds-number turbulence is associated with weak dissipation, when B_0 is large. The apparent paradox is resolved as follows: the equation for the energy decay is obtained in the usual way by dotting $\mathbf{v}$ with (2.3), $\mathbf{b}$ with (2.4), adding, integrating over the domain and using periodicity. The result is

$$\frac{\partial E}{\partial t} = -3\nu_{\rm ion} \int {\rm dV} \left(\frac{\partial v_z}{\partial z}\right)^2 . \tag{4.1}$$

Viscous dissipation therefore depends only on parallel gradients of v_z. As has been suggested previously (Shebalin *et al.* 1983; Carbone and Veltri 1990; Oughton *et al.* 1994), and will also be seen below, when B_0 is large the nonlinear dynamics are such that spectral transfer of $\mathbf{v}$ and $\mathbf{b}$ in the parallel direction is suppressed. The two effects – ion parallel dissipation and reduced spectral transfer parallel to B_0 – thus combine to keep the right-hand side of (4.1) small.

Simulation results support these arguments as shown in Fig. 3, which displays contour plots of $\log|v_z(k_\perp, k_\parallel)|^2$ and $\log|v_x(k_\perp, k_\parallel)|^2$ for run 07 ($k_\parallel = \mathbf{k} \cdot \hat{\mathbf{B}}_0$, $k_\perp^2 = k^2 - k_\parallel^2$). The isotropic nature of the initial conditions is deposed in less than

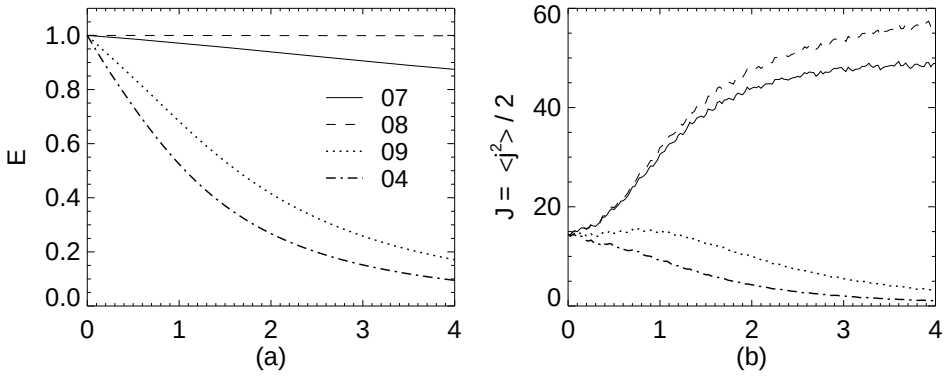

Figure 2. Time histories for some global quantities. (a) total fluctuation energy; (b) mean-square current density. [The horizontal coordinate is time.]

a turnover time, and it is clear that parallel spectral transfer is inhibited. Note that the $k_\perp$ dependence has been averaged over all orientations of wave vectors with given k and $k_\parallel$.

The situation is quite different when the resistivity is non-zero – even at the $\eta/\nu_{\rm ion} \sim 10^{-3}$ level (run 09). Energy dissipation rates are then restored to values much closer to those seen in runs with the standard Laplacian viscous and resistive terms, such as run 04 (hereafter 'standard dissipative' runs) (Shebalin *et al.* 1983; Oughton *et al.* 1994). The reason for this is clear: when $\eta \neq 0$, enhanced spectral transfer in the perpendicular direction cannot circumvent dissipation of E^b because the resistive term is isotropic in k-space. Furthermore, Alfvén-effect activity (see below) means that dissipation of E^b is followed by a transfer of kinetic energy into magnetic energy (to maintain equipartition), which is then subject to resistive dissipation. Thus, this coupling leads indirectly to *resistive* decay of the *velocity* fluctuations.

Analogous differences between the η zero and non-zero cases are observed in the evolution of the mean-square current density, $J = \langle \frac{1}{2}|\mathbf{j}|^2 \rangle$ (Fig. 2*b*), and the enstrophy, $\Omega = \langle \frac{1}{2}|\boldsymbol{\omega}|^2 \rangle$ (not shown), which behave very similarly. Zero-resistivity runs are associated with $J(t)$ and $\Omega(t)$ profiles which grow for a few turnover times and then level out at an approximately constant value (which decreases as $\nu_{\rm ion}$ increases). This is qualitatively the same behaviour observed in ideal runs. Such similarity suggests that absolute equilibrium predictions (Stribling and Matthaeus 1990) may be of relevance to these flows, a conjecture which is the object of further research. By contrast, $\eta \neq 0$ runs show at most only slight increases in J and Ω, followed by more or less monotonic decay. Again, this behaviour is very similar to that observed in 'standard dissipative' runs. As far as bulk properties are concerned it is apparent that even a small resistivity is enough to swamp the gentler $\nu_{\rm ion}$ decay effects.

For $\eta = 0$ runs the kinetic energy is, to a good approximation, equal to the magnetic, as would be expected on the basis of the Alfvén effect (Kraichnan 1965; Pouquet *et al.* 1976). This postulates that in the presence of a strong large-scale magnetic field, $\mathbf{v}$ and $\mathbf{b}$ fluctuations behave like Alfvén waves, and thus involve an inherent equipartition of kinetic and magnetic energy, on average. The approximate equality of J and Ω is an immediate consequence of the Alfvén effect holding mode

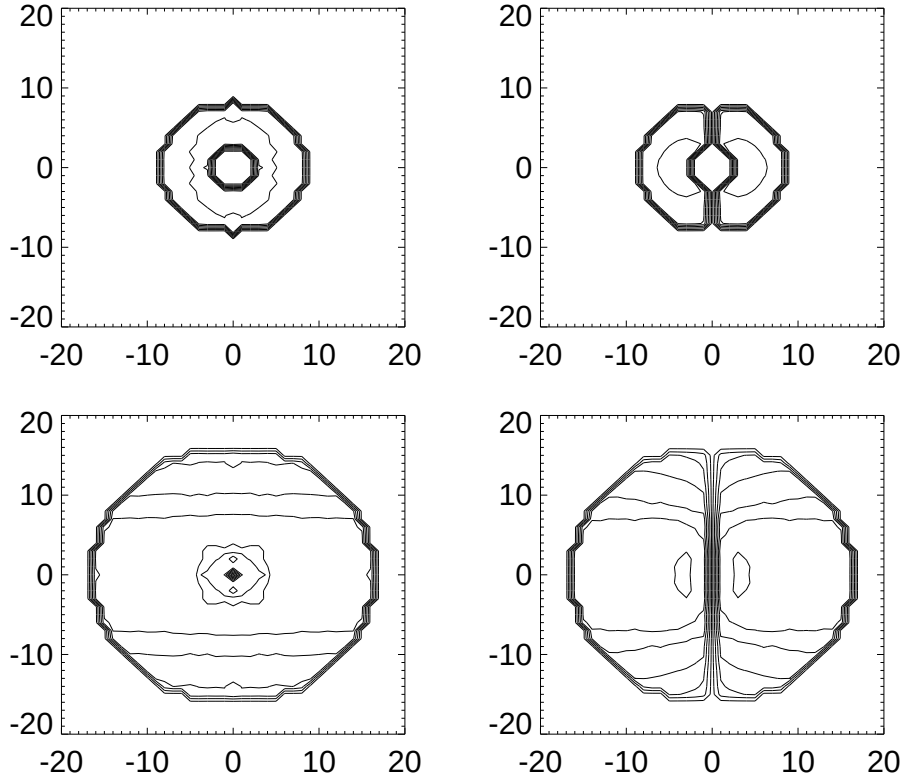

Figure 3. Contour plots for the logarithms of $|v_x(k_\perp, k_\parallel)|^2$ (left-hand side) and $|v_z(k_\perp, k_\parallel)|^2$ (right-hand side). Data are for run 07 at $t = 0$ (top row) and $t = 1.4$ (bottom row). The spectra for the x and z components appear significantly different along the $k_\perp = 0$ axis only because of the way the incompressibility constraint, $\mathbf{k} \cdot \mathbf{v}(\mathbf{k}) = 0$, and the $k_\perp$, $k_\parallel$ decomposition interact. [The horizontal axis is $k_\perp$ and the vertical $k_\parallel$.]

by mode. The resistive runs, however, evolve to give an excess of kinetic energy ($r_A = E^v/E^b \approx 1.2$ at $t = 4$). We suggest that this is a consequence of the isotropic resistive dissipation being stronger than the anisotropic viscous decay. While $\mathbf{v}$ and $\mathbf{b}$ are manifestly coupled, there is evidently a lag in transferring excitations from the kinetic to the magnetic components. The effect is also present in the linear runs and we are investigating the dynamics of this case in an effort to improve understanding of the process.

Linear runs have E, J, and Ω profiles which are of course strictly monotonic decreasing (not shown). In the case of run 17, the decrease is so slow that it is graphically undetectable. This lack of any significant evolution is characteristic of all the linear runs performed with $\eta = 0$ and $\nu_{\rm ion} \lesssim 10^{-1}$.

4.2. Spectral Anisotropy

Spectral anisotropy concerns the 'energy' distribution as a function of wave vector, as distinct from wavenumber. A useful way of quantifying it was introduced by Shebalin *et al.* (1983); see also Carbone and Veltri (1990) and Oughton *et al.*(1994). Given a field $\mathbf{Q}(\mathbf{x}, t)$ with Fourier transform $\mathbf{Q}(\mathbf{k}, t)$, the anisotropy angle θ_Q is

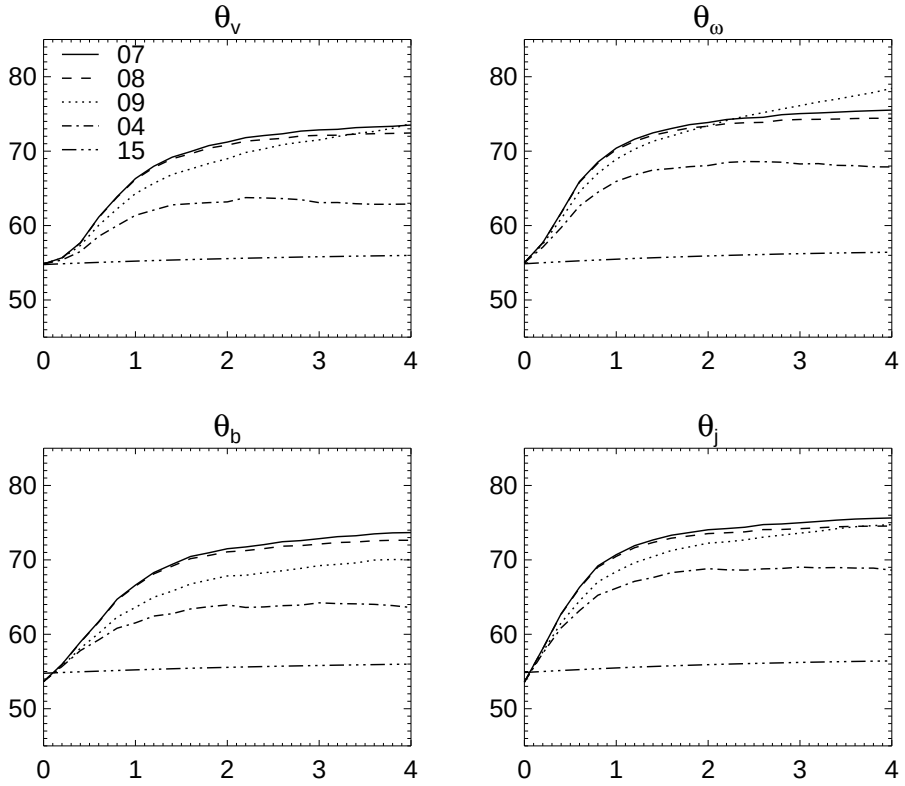

Figure 4. Time histories of some anisotropy angles. [Angles are in degrees.]

defined by

$$\tan^2\theta_Q = \frac{\Sigma\, k_\perp^2 |\mathbf{Q}(\mathbf{k},t)|^2}{\Sigma\, k_z^2 |\mathbf{Q}(\mathbf{k},t)|^2}, \tag{4.2}$$

where the sums are over all retained wavevectors $\mathbf{k}$. Here we concentrate on $\mathbf{Q}$s such as $\mathbf{v}$, $\boldsymbol{\omega}$, $\mathbf{b}$, $\mathbf{j}$, and the $\mathbf{e}_1$, $\mathbf{e}_2$ polarizations of $\mathbf{v}$ and $\mathbf{b}$. Examination of (4.2) indicates that $\tan\theta_Q$ is interpretable as the ratio of (weighted) RMS wavenumbers computed parallel and perpendicular to $\mathbf{B}_0$. It is straightforward to show that an isotropic spectrum has $\theta_Q = \tan^{-1}\sqrt{2} \simeq 55°$, while 2D spectra (meaning ones where the excited modes have $\mathbf{k} \perp \mathbf{B}_0$) have $\theta_Q = 90°$.

Plots of θ_v and θ_ω for five representative runs are displayed in Fig. 4. Although the angles fluctuate slightly, the overall trend is a monotonic increase with time, initially quite a rapid one. In fact, these two angles increase with time for all the nonlinear (and most of the linear) runs listed in table 1, but the level attained depends on the specific run parameters. In general, the anisotropy increases as $\nu_{\rm ion}$ increases, although the effect is rather weak. This is at least partially a consequence of $\alpha = 2B_0/3k\nu_{\rm ion}$ being greater than unity for most of the runs (Table 1). As shown in Sec. 3, anisotropy associated with $\nu_{\rm ion}$ only develops (linearly) if $\alpha < 1$. The simulation results are in accord with this prediction, and also with the prediction of increasing anisotropy with decreasing α. Discussion of the anisotropy results for linear runs is deferred to Sec. 4.2.1.

The anisotropy angles for the ideal run (06) are almost identical to those of run 08, with $\eta = 0$, $\nu_{\rm ion} = 10^{-1}$, indicating that the bulk of the anisotropy is generated

by the nonlinear process first discussed in connection with 'standard dissipation' runs (Shebalin *et al.* 1983; Oughton *et al.* 1994). However, $\eta = 0$ runs with $\alpha < 1$ produce spectral anisotropies which are slightly enhanced with respect to the ideal run values. We return to this point below.

The angles θ_b and θ_j generally behave very similarly to their velocity counterparts. In particular, when $\eta = 0$, θ_v and θ_b are essentially identical, and likewise θ_ω and θ_j. For $\eta \neq 0$, we typically observe $\theta_v \geq \theta_b$, and $\theta_\omega \geq \theta_j$ after $t \approx 1$, with the margin being 3°–4°. We believe that this, like the excess of kinetic energy, is a consequence of the resistive dissipation being stronger than the viscous: resistivity reduces the level of magnetic excitation everywhere in k-space, whereas $\nu_{\rm ion}$ effects are weaker and also directionally selective. As a result the **v**–**v** nonlinear couplings are likely to be the strongest, leading to stronger anisotropies in **v** compared with **b**.

Figure 4 also contains information about the scale dependence of the anisotropy. At any fixed time, each run is such that $\theta_\psi < \theta_v < \theta_\omega$ and $\theta_a < \theta_b < \theta_j$, with $\boldsymbol{\psi}$ and **a** respectively the velocity stream function and magnetic vector potential. The same behaviour was observed in simulations of the 'standard dissipation' MHD equations (Shebalin *et al.* 1983; Oughton *et al.* 1994). Since **v** depends more strongly on the small scales than $\boldsymbol{\psi}$, and $\boldsymbol{\omega}$ even more so, the θ behaviour is interpreted as evidence for spectral anisotropy being stronger at smaller scales. Note, however, that shell-model work (Carbone and Veltri 1990) indicates spectral anisotropy is approximately uniform throughout a well-developed inertial range. Unfortunately, direct numerical simulation of 3D MHD flows with a substantial inertial range is not yet routinely feasible.

4.2.1. Polarization effects. We turn now to connections between the fluctuation polarizations and spectral anisotropy, considering first the linear runs. As shown in Sec. 3, only the $\mathbf{e}_2$ polarization is (directly) affected by the value of $\nu_{\rm ion}$, and the spectral anisotropy should increase only for this polarization. Figure 5 shows plots of the anisotropy angles and energies for the two polarization components of **v** and **b**. In agreement with the theory for $\eta = 0$ runs, only the $\mathbf{e}_2$ components of run 15 show any evolution: decay for the energies and growth for the angles. The magnetic quantities are graphically indistinguishable from their kinetic counterparts, although small differences do in fact exist between the $\mathbf{e}_2$ components. This behaviour is in complete accord with the linear theory (Oughton 1996).

Resistive runs behave somewhat differently. Both polarization components of the energies decay, and the magnetic behaviour is now clearly distinct from the kinetic. Specifically, the $\mathbf{e}_1$ and $\mathbf{e}_2$ components of E^b decay faster than those of E^v, but in each case the $\mathbf{e}_2$ component decays more. The magnetic energy decays faster because the resistive dissipation is isotropic and considerably stronger than the viscous dissipation. The situation is even more interesting for the anisotropy angles. The $\mathbf{e}_1$ and $\mathbf{e}_2$ angles for **v** *both* increase, whereas those for **b** decrease slightly. Moreover, the growth of the **v** angles is significantly greater than that seen in run 15 (figure 5). An explanation of this behaviour is given in the next paragraph.

It can be shown (Oughton 1996) from the linear equations that components of the $\mathbf{e}_1$ energy spectra obey the following equations

$$\frac{\mathrm{d}}{\mathrm{d}t}|\psi_1(\mathbf{k})|^2 = -2(\mathbf{k}\cdot\mathbf{B}_0)^2 H_1, \tag{4.3}$$

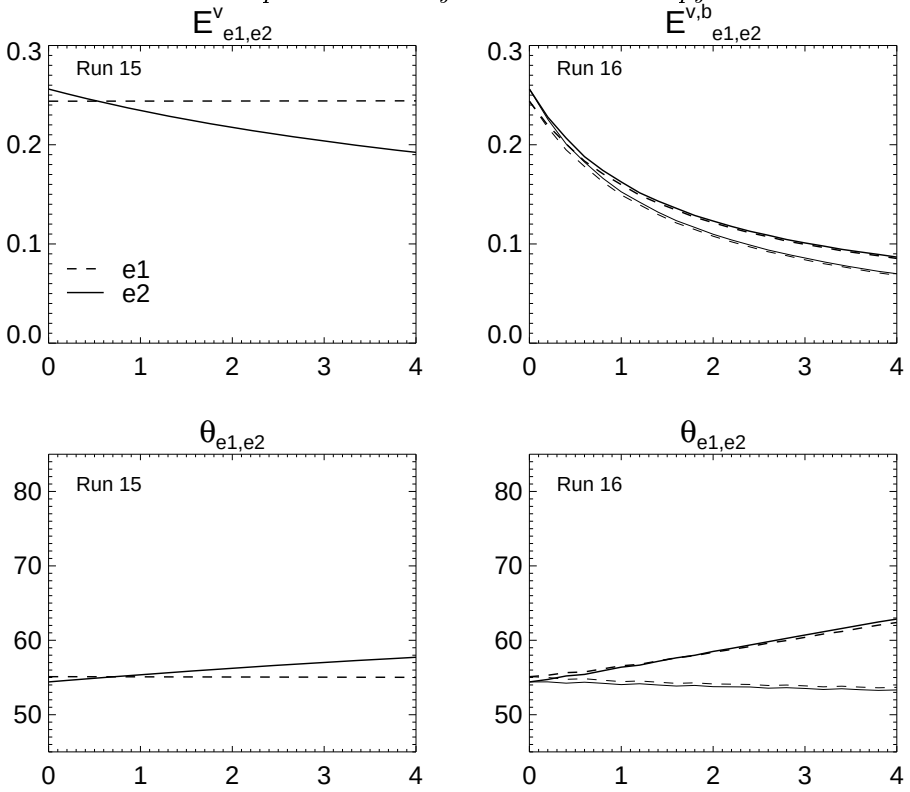

Figure 5. Time histories in terms of the $\mathbf{e}_1$ and $\mathbf{e}_2$ polarization components of $\mathbf{v}$ and $\mathbf{b}$ for the linear runs 15 and 16. Top: kinetic and magnetic energies. Bottom: anisotropy angles. Thick (thin) curves represent velocity (magnetic) field quantities.

$$\frac{\mathrm{d}}{\mathrm{d}t}|a_1(\mathbf{k})|^2 = \quad 2(\mathbf{k}\cdot\mathbf{B}_0)^2 H_1 - 2\eta k^2\,|a_1(\mathbf{k})|^2, \tag{4.4}$$

where $H_1 \propto \mathrm{Im}\{\psi_1^* a_1\}$ is non-negative and oscillates with decreasing amplitude. The decay of $|\psi_1(\mathbf{k})|^2$ is therefore anisotropic with parallel wavevector modes being more strongly damped. Hence the associated anisotropy angle will be quasi-2D, as shown in Fig. 5. For the magnetic energy there is an equal and opposite effect (plus resistive damping), leading to an enhancement of energy in parallel modes and a consequent decrease of θ^b_{e1}. A similar situations holds for the $\mathbf{e}_2$ components but with the addition of ν_{ion} dissipation effects. While the physical nature of H_1 and H_2 is not completely understood, they are related to the 'helicity of the electric field' (Zhou and Matthaeus 1990).

The nonlinear results parallel the linear ones, provided the much stronger nonlinear anisotropy generation process is taken into account (Fig. 6). In all cases, the $\mathbf{e}_2$ polarization is more anisotropic than the $\mathbf{e}_1$ one for a given field. When $\nu_{\mathrm{ion}} \lesssim 10$, however, the difference is often less than a degree. Table 1 shows that $\alpha > 1$ for such runs, and thus the propagation condition (3.3) is satisfied for all retained wavenumbers. Consequently no anisotropy can develop via this mechanism. Of course, for large enough wavenumbers, α is always less than unity and ion parallel anisotropy is expected to develop at these scales. Simulations covering a larger range of scales are clearly called for.

Figure 6 also shows that the $\mathbf{e}_1$ and $\mathbf{e}_2$ polarizations of $\mathbf{v}$ both decay at approx-

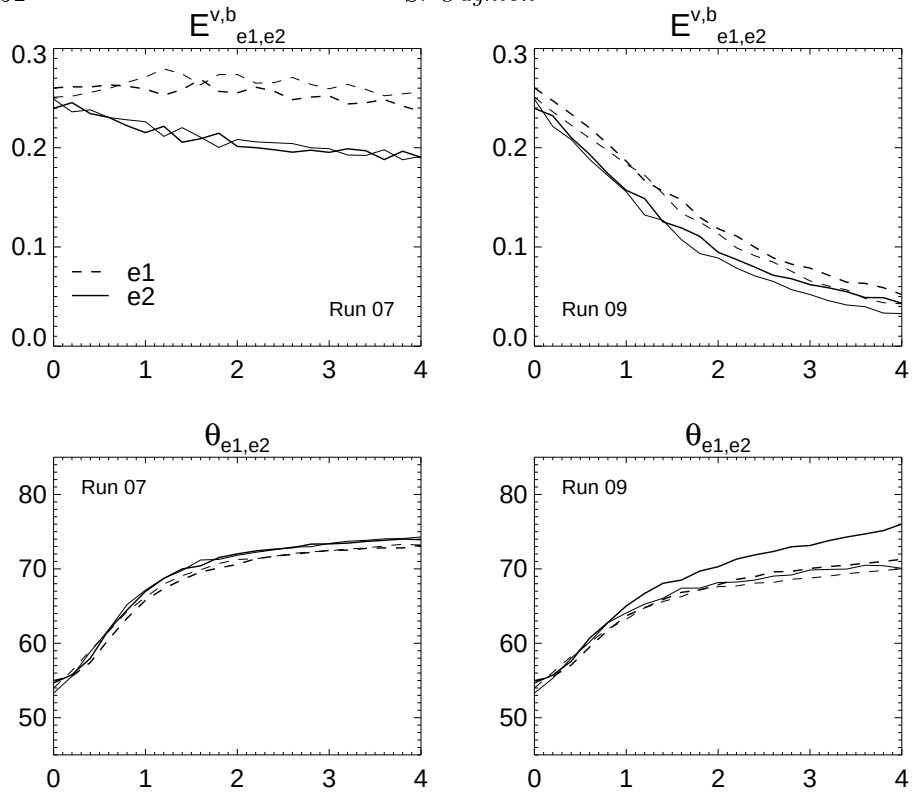

Figure 6. Same as Fig. 5, except for the nonlinear runs 07 and 09.

imately the same rate for a given nonlinear run. Since for the $\eta = 0$ runs only the $\mathbf{e}_2$ polarization has a direct dissipative channel, nonlinear couplings must be inducing a fairly rapid transfer of excitation between the two polarizations. This is easily confirmed by substituting (3.4) and its magnetic counterpart into the Fourier transform of (2.3)–(2.5) and forming scalar products with $\mathbf{e}_1$ and $\mathbf{e}_2$.

Shell model work using 'standard dissipation' terms (Carbone and Veltri 1990) reveals a small polarization dependence in the anisotropy angles, suggesting that the nonlinear anisotropy generation mechanism also has a weak polarization dependence. While we do not observe such an effect in runs 04 and 06, this may be because the Reynolds numbers employed are too small to achieve sustained strong turbulence. Assuming that the polarization dependence is not an artifact of the shell model itself, this compounds the difficulty of estimating the polarization dependence of the anisotropy angles as a function of $\nu_{\rm ion}$.

A few comments regarding the temporal persistence of the anisotropy are apposite. Simulations employing 'standard dissipative' terms (Shebalin *et al.* 1983; Oughton *et al.* 1994) and $B_0 \approx 1$ revealed that the anisotropy angles θ first grow and then level out. On the other hand, non-dissipative runs using the same initial conditions produce essentially identical θs for the first few turnover times, but thereafter decay back towards the isotropic value on a much longer timescale (see Fig. 10 of Shebalin *et al.* 1983). This was argued to be a consequence of the statistical mechanics appropriate for such absolute equilibrium flows (Kraichnan and Montgomery 1980; Stribling and Matthaeus 1990), where the energy attempts to equipartition itself amongst all retained wave-*vector* modes. Here, however, we find

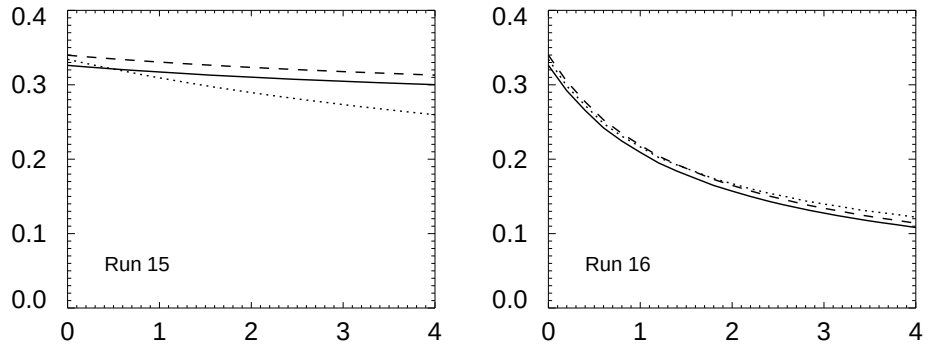

Figure 7. Time histories of the velocity field variances for two linear runs. Solid $\langle v_x^2 \rangle$, dashed $\langle v_y^2 \rangle$, dotted $\langle v_z^2 \rangle$.

no such ideal decay of the θs, even though the ideal run 06 has been followed out to $t \approx 40$. The anisotropy angles remain roughly constant for $t \gtrsim 5$.

In order for the absolute equilibrium predictions to be relevant, enough time must have passed for all modes to equilibrate. The large scales will be the slowest to do so, taking several spectral transfer times, τ_s. In the Kraichnan (1965) approach $\tau_s = \tau_{NL}^2/\tau_A \approx k_0 B_0/(k_0 u_{\rm rms})^2$ which is approximately 10 turnover times in our case (τ_{NL} and τ_A are respectively the nonlinear and Alfvén timescales). On the basis of this argument we therefore expect to see evidence for the θs returning to the isotropic value by $t \approx 40$. It appears that large B_0 causes the spectral anisotropy to persist long after absolute equilibrium theory (with just E and H_c as invariants) predicts its demise. One might speculate that the small but non-zero magnetic helicity is inducing back-transfer of excitations (Frisch *et al.* 1975; Stribling and Matthaeus 1990) and somehow thwarting the return to isotropy.

Corrected the exponent error which appears in the published version.

4.3. Variance Anisotropy

We denote the variance of the x components of $\mathbf{v}(\mathbf{x})$ and $\mathbf{b}(\mathbf{x})$ by $\langle v_x^2 \rangle$ and $\langle b_x^2 \rangle$, and similarly for the other components. It will often be convenient to work with the *relative variances*, $\langle v_x^2 \rangle / \langle v_z^2 \rangle$, etc., where the z-variance is always used as the normalising factor.

4.3.1. Linear runs. Recall that the linear theory of Sec. 3 indicated that for $\eta = 0$, $\nu_{\rm ion} \neq 0$ runs, the z components should decay faster than the others, since the former are purely $\mathbf{e}_2$-polarized while the latter (in general) also include $\mathbf{e}_1$ components, and these are immune to the viscous decay. The left-hand panel of Fig. 7 shows that this is indeed the case for the velocity variances of run 15 (magnetic variances behave almost identically). The associated relative variances increase approximately linearly with time from unity to about 1.2 at $t = 4$. All linear runs with $\alpha < 1$ and $\eta = 0$ display similar behaviour, with the effect becoming stronger as α decreases.

For runs with $\eta = 10^{-2}$, however, the resistive decay dominates and all three components of the variances decay much faster than in the analogous $\eta = 0$ case (Fig. 7). While at first sight the decay rates look roughly the same, closer examination reveals that the relative magnetic variances still tend to increase with time, but the velocity ones actually decrease. Recall that for such runs E^b decays faster than E^v, and we have argued that this is due to the stronger (and isotropic) nature

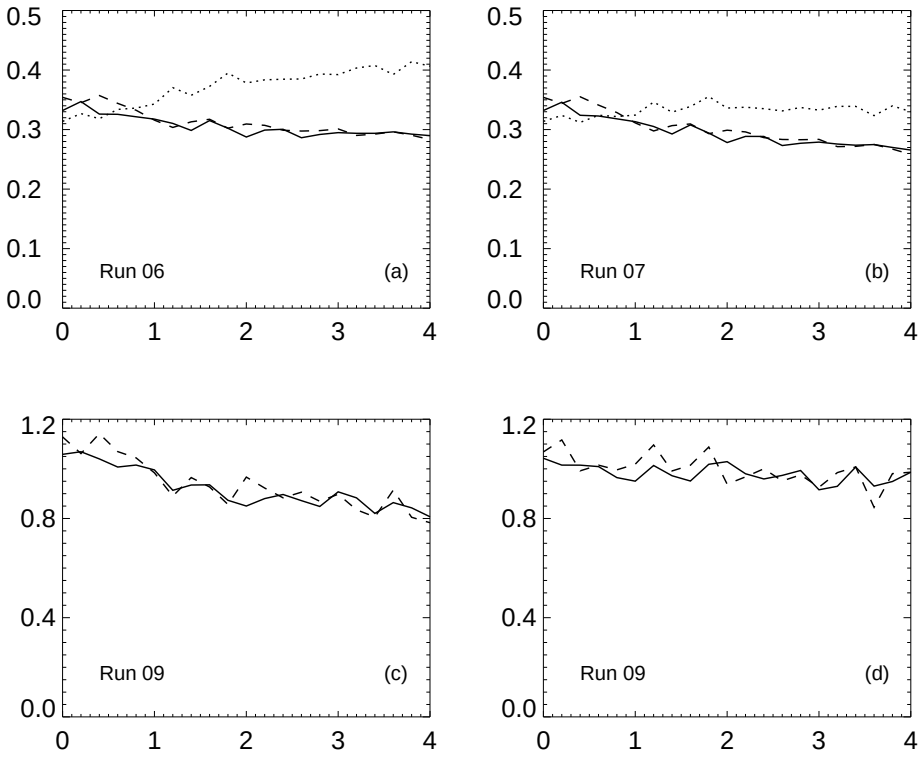

Figure 8. Variance time histories for three nonlinear runs. (a, b) Velocity variances; solid $\langle v_x^2 \rangle$, dashed $\langle v_y^2 \rangle$, dotted $\langle v_z^2 \rangle$. (c) Relative velocity variances; solid $\langle v_x^2 \rangle / \langle v_z^2 \rangle$, dashed $\langle v_y^2 \rangle / \langle v_z^2 \rangle$. (d) Same as (c) except for the relative magnetic variances.

of the resistive dissipation (cf. Fig. 5). Evidently, however, ion parallel effects are preserving $\langle v_z^2 \rangle$, relatively speaking, but not $\langle b_z^2 \rangle$.

4.3.2. Nonlinear runs. Figure 8(a) shows plots of the velocity variances for the non-dissipative run 06 (magnetic variance profiles are very similar). Clearly when nonlinear interactions are present, the 'natural' state of the relative variances is significantly less than unity, due to transfer of energy from the x and y components to the z component.

The preferential decay of the z components for runs with $\eta = 0$ and $\nu_{\rm ion} \neq 0$ reduces the dominance of $\langle v_z^2 \rangle$ and $\langle b_z^2 \rangle$, causing the relative variances to increase above the 'natural' levels but still remain less than unity (Fig. 8b). One objective of this work was to determine if ion parallel viscosity effects could produce excess power in the perpendicular directions, as observed in the solar wind (Klein *et al.* 1991; Horbury *et al.* 1995). While no nonlinear simulations have been performed where the relative variances evolve to levels significantly above unity, it seems possible that this will occur for sufficiently small α, as in the linear runs.

Inclusion of the resistive term has little effect on the relative velocity variances, but tends to further increase the magnetic ones above their 'natural' levels (Figs 8c,d). This is similar to the behaviour of the analogous linear runs, and analytic work on the linear dynamics is being undertaken in an attempt to improve

understanding here. At present we do not have adequate explanations for several of the variance anisotropy features as a function of the dissipation coefficients.

5. Summary and Conclusions

The results presented above indicate that when B_0^2 is much larger than the energy in the fluctuations, nonlinear 3D MHD flows are associated with anisotropic spectral transfer, with a suppression of transfer for wave-vector modes quasi-parallel to B_0. Measured in terms of anisotropy angles, or equivalently ratios of perpendicular and parallel correlation lengths, the anisotropies tend to increase with both wavenumber and time. This dynamic evolution towards weakly coupled planes of two-dimensional turbulence (with their normals parallel to $\hat{\mathbf{B}}_0$) was also seen in nonlinear simulation studies employing 'standard dissipation' terms (Shebalin *et al.* 1983; Oughton *et al.* 1994). Linear runs are also associated with increasing spectral anisotropy when $\alpha = 2B_0/3k\nu_{\rm ion} < 1$, with a strong polarization dependence when $\eta = 0$, only the $\mathbf{e}_2$ polarizations of $\mathbf{v}$ and $\mathbf{b}$ being affected. The polarization dependence is much weaker when $\eta \neq 0$ and also in the nonlinear runs, for which the two polarizations no longer evolve independently.

Perhaps the most important conclusion to be drawn from this work is that even when the resistivity is vastly smaller than the ion parallel viscosity, it can still provide the dominant method of dissipation and significantly affect the spectral and variance anisotropy levels. This stands as a further warning regarding the neglect of 'small' terms that involve spatial gradients.

In the nonlinear case the spectral anisotropy appears to be a composite of behaviour due to two distinct processes: (1) anisotropy generation by the nonlinear couplings, which is ideal in the sense that dissipation is required only for the persistence of the anisotropy, not the development, and is already well reported (Shebalin *et al.* 1983; Oughton *et al.* 1994); and (2) anisotropy associated with the (linear) ion parallel viscosity dissipation. Since the latter process is linear and weak compared to the former, we might expect the two effects to be roughly additive. Indeed, we find that $\theta_v^{07} \approx \theta_v^{06} + \theta_v^{15} - 55°$, where the superscripts denote run numbers. Of course, this is just one example and if higher wavenumber modes are excited, the ion parallel viscosity effect will become more important in determining the net anisotropy. In such cases it seems less likely that the effects will be additive. Both processes require a strong background magnetic field, but whereas the nonlinear mechanism appears to saturate when $B_0 \gtrsim 3$ (Shebalin *et al.* 1983; Oughton *et al.* 1994), the ion parallel mechanism gets weaker as B_0 is increased, and in fact turns off for $\alpha > 1$.

Variance anisotropy is also subject to $\nu_{\rm ion}$ effects. As α decreases below unity the x and y components of the kinetic and magnetic energies become more substantial compared to the z components. In the linear runs the former become dominant, largely because of the preferential decay of the latter. In nonlinear runs it is the z components which are predominant, but less and less so as α decreases. Indeed, it is possible that at small enough α (e.g. large enough k), the x and y components will become dominant.

For both spectral and variance anisotropy there is a strong similarity between the results discussed here and those reported in 2D and 3D simulation studies using 'standard dissipation' terms (Shebalin *et al.* 1983; Carbone and Veltri 1990; Oughton *et al.* 1994). When analysing observational data, such as that obtained

from spacecraft measurements in the solar wind, this similarity is likely to make it difficult to extract information regarding the relative importance of the nonlinear and ion parallel anisotropy generation processes.

This work was originally motivated by its possible relevance to interplanetary fluctuations. However, the solar wind is an almost collisionless plasma, so that there are questions as to the relevance of the Braginskii transport coefficients (Montgomery 1992). Furthermore, it is rare to find intervals of solar wind data where the mean magnetic field is much greater than the fluctuating one. In fact, often $E^b/B_0 > 1$ over the solar poles (Horbury *et al.* 1995), so that the simulations discussed here are for a different parameter regime. Nonetheless, they may be relevant for small enough scales in the solar wind, since the fluctuation energy at these scales will indeed be much less than that in the mean field. In particular, observed relative variance anisotropies (Klein *et al.* 1991; Horbury *et al.* 1995) are greater than unity and increase with decreasing scale. This is in qualitative agreement with the linear theory and simulations. Unfortunately, nonlinear couplings tend to swamp or perhaps even destroy the linear effects so that their relevance is questionable given the prevailing belief that solar wind fluctuations are turbulent. On the other hand, these simulations have a limited range of scales excited, and it may be that the linear effects re-emerge at smaller scales.

We close by noting that the anisotropy levels reported here show significant dependence on the (modest) Reynolds numbers, or in other words are affected by the strength of the turbulence. Since higher Reynolds numbers will lead to longer periods of fully developed turbulence it is expected that the anisotropy levels will rise with increasing Reynolds numbers (Shebalin *et al.* 1983; Oughton *et al.* 1994), perhaps saturating at very large Reynolds numbers (Carbone and Veltri 1990). Higher resolution simulations will allow investigation of these conjectures.

Acknowledgements

We wish to thank D. Montgomery for valuable comments and the suggestion to work on this problem. This work was supported in part by grant SCI/180/94/400 from the Nuffield Foundation, and the UK PPARC grant GR/K98711.

References

Batchelor, G. K. 1970 *The Theory of Homogeneous Turbulence.* Cambridge University Press.

Bavassano, B., Dobrowolny, M., Fanfoni, G., Mariani, F. and Ness, N. F. 1982 Statistical properties of MHD fluctuations associated with high-speed streams from Helios-2 observations. *Solar Phys.* **78**, 373.

Belcher, J. W. and Davis Jr., L. 1971 Large-amplitude Alfvén waves in the interplanetary medium, 2. *J. Geophys. Res.* **76**, 3534.

Bieber, J. W., Wanner, W. and Matthaeus, W. H. 1996 Dominant two-dimensional solar wind turbulence with implications for cosmic ray transport. *J. Geophys. Res.* **101**, 2511.

Book, D. L. 1987 *NRL Plasma Formulary.* Washington, DC: NRL Publication 0084-4040.

Braginskii, S. I. 1965 Transport processes in a plasma. *Rev. Plasma Phys.* (ed. M. A. Leontovich), p. 205. Consultants Bureau, New York.

Carbone, V. and Veltri, P. 1990 A shell model for anisotropic magnetohydrodynamic turbulence. *Geophys. & Astrophys. Fluid Dyn.* **52**, 153.

Frisch, U., Pouquet, A., Léorat, J. and Mazure, A. 1975 Possibility of an inverse cascade of magnetic helicity in magnetohydrodynamic turbulence. *J. Fluid Mech.* **68**, 769.

Horbury, T., Balogh, A., Forsyth, R. J. and Smith, E. J. 1995 Anisotropy of inertial range turbulence in the polar heliosphere. *Geophys. Rev. Lett.* **22**, 3405.

Klein, L. W., Roberts, D. A. and Goldstein, M. L. 1991 Anisotropy and minimum variance directions of solar wind fluctuations in the outer heliosphere. *J. Geophys. Res.* **96**, 3779.

Kraichnan, R. H. 1965 Inertial-range spectrum of hydromagnetic turbulence. *Phys. Fluids* **8**, 1385.

Kraichnan, R. H. and Montgomery, D. C. 1980 Two-dimensional turbulence. *Rept. Prog. Phys.* **43**, 547.

Lesieur, M. 1990 *Turbulence in Fluids*, 2nd edn. Kluwer, Dordrecht.

Matthaeus, W. H. and Goldstein, M. L. 1982 Measurement of the rugged invariants of magnetohydrodynamic turbulence in the solar wind. *J. Geophys. Res.* **87**, 6011.

Matthaeus, W. H., Goldstein, M. L. and Roberts, D. A. 1990 Evidence for the presence of quasi-two-dimensional nearly incompressible fluctuations in the solar wind. *J. Geophys. Res.* **95**, 20 673.

Matthaeus, W. H., Ghosh, S., Oughton, S. and Roberts, D. A. 1996 Anisotropic three-dimensional MHD turbulence. *J. Geophys. Res.* **101**, 7619–7629.

Moffatt, H. K. 1967 On the suppression of turbulence by a uniform magnetic field. *J. Fluid Mech.* **28**, 571.

Montgomery, D. C. 1992 Modifications of magnetohydrodynamics as applied to the solar wind. *J. Geophys. Res.* **97**, 4309.

Montgomery, D. C. and Matthaeus, W. H. 1995 Anisotropic modal energy transfer in interstellar turbulence. *Astrophys. J.* **447**, 706.

Montgomery, D. C. and Turner, L. 1981 Anisotropic magnetohydrodynamic turbulence in a strong external magnetic field. *Phys. Fluids* **24**, 825.

Orszag, S. A. 1977 Lectures on the statistical theory of turbulence. *Fluid Dynamics. Les Houches Summer School* (ed. R. Balian and J.-L. Peube), 1973, p. 235. New York: Gordon and Breach, New York.

Oughton, S. 1996 Energy dynamics in linear MHD with ion parallel viscosity. Submitted to *J. Plasma Phys.*

Oughton, S., Matthaeus, W. H. and Ghosh, S. 1995 Anisotropy in incompressible and compressible 3D MHD turbulence. *Small-Scale Structures in Three-Dimensional Hydro and Magnetohydrodynamic Turbulence. Nice Workshop, January 1995* (ed. M. Meneguzzi, A. Pouquet and P.L. Sulem), p. 273. Lecture Notes in Physics, Vol 462, Springer-Verlag, Berlin.

Oughton, S., Priest, E. R. and Matthaeus, W. H. 1994 The influence of a mean magnetic field on three-dimensional MHD turbulence. *J. Fluid Mech.* **280**, 95–117.

Pouquet, A., Frisch, U. and Léorat, J. 1976 Strong MHD helical turbulence and the nonlinear dynamo effect. *J. Fluid Mech.* **77**, 321.

Robinson, D. and Rusbridge, M. 1971 Structure of turbulence in the zeta plasma. *Phys. Fluids* **14**, 2499.

Shebalin, J. V., Matthaeus, W. H. and Montgomery, D. 1983 Anisotropy in MHD turbulence due to a mean magnetic field. *J. Plasma Phys.* **29**, 525.

Sridhar, S. and Goldreich, P. 1994 Toward a theory of interstellar turbulence: I. Weak Alfvénic turbulence. *Astrophys. J.* **432**, 612.

Stribling, T. and Matthaeus, W. H. 1990 Statistical properties of ideal three-dimensional magnetohydrodynamics. *Phys. Fluids B* **2**, 1979.

Stribling, T., Matthaeus, W. H. and Ghosh, S. 1994 Nonlinear decay of magnetic helicity in magnetohydrodynamics with a mean magnetic field. *J. Geophys. Res.* **99**, 2567.

Stribling, T., Matthaeus, W. H. and Oughton, S. 1995 Magnetic helicity in magnetohydrodynamic turbulence with a mean magnetic field. *Phys. Plasmas* **2**, 1437–1452.

Zhou, Y. and Matthaeus, W. H. 1990 Transport and turbulence modeling of solar wind fluctuations. *J. Geophys. Res.* **95**, 10 291.

Zweben, S., Menyuk, C. and Taylor, R. 1979 Small-scale magnetic fluctuations inside the macrotor tokamak. *Phys. Rev. Lett.* **42**, 1270.